Chemical Engineering Science 95 (2013) 301–312

Contents lists available at SciVerse ScienceDirect

Chemical Engineering Science

journal homepage: www.elsevier.com/locate/ces

Electrochemical behaviour of aluminium in electrocoagulation processes

Martin Mechelhoff [a,1], Geoff H. Kelsall [a], Nigel J.D. Graham [b,*]

[a] Department of Chemical Engineering, Imperial College London, London SW7 2AZ, United Kingdom
[b] Department of Civil and Environmental Engineering, Imperial College London, London SW7 2AZ, United Kingdom

HIGHLIGHTS

- Electrochemical behaviour of Al electrodes in electrocoagulation processes studied.
- Important role of solution chemistry and electrode surface roughness on passivation.
- Humic acid attenuated the depassivating effect of chloride ions.
- Freshly roughened electrode surfaces exhibited spontaneous depassivation.
- Reactor model predicted lower pH (5.5) at anode surfaces than in bulk solution (7).

ARTICLE INFO

Article history:
Received 21 December 2012
Received in revised form
4 March 2013
Accepted 6 March 2013
Available online 26 March 2013

Keywords:
Electrochemistry
Coagulation
Chemical processes
Separations
Aluminium dissolution
Passivation

ABSTRACT

Passivation of aluminium electrodes is a common problem in electrocoagulation reactors used for the purification of natural waters, leading to high cell voltages and compromising the viability of such industrial processes. In order to identify possible mitigation strategies, cyclic voltammetric, potentiostatic and galvanostatic measurements were made to investigate the effects of electrode surface topography and solution composition on the electrochemical behaviour of pure aluminium and Al 1050 in neutral electrolyte solutions. In addition, electrochemical impedance spectroscopy was used to estimate thicknesses of passive layers before and after dissolution. Chloride ions, well-known pitting promoters, were found to facilitate dissolution of passive surfaces, though attenuated by the presence of the naturally-occurring contaminant humic acid. Under galvanostatic conditions, a smooth aluminium electrode showed a constant rise in electrode potential due to passivation. However, even in the absence of pitting promoters electrodes with a 'rough' surface finish (R_a-values $> 1\ \mu m$) exhibited an initial potential increase, followed by a dramatic decrease to relatively low steady state values due to 'spontaneous de-passivation'. The precipitation of dissolved aluminium(III), releasing H^+ ions, was identified as the probable cause of this effect, leading to acidic pH values, locally dissolving the passive layer and enhancing dissolution rates.

1. Introduction

Electrocoagulation is a water purification process that uses electrical energy to dissolve metals, such as aluminium and iron, to destabilise colloidal suspensions resulting in the flocculation of contaminants. It obviates the need for additions of aqueous solutions of Al^{III} or Fe^{III} coagulants, required by conventional chemical coagulation methods, as used for purifying potable water.

The feasibility of applying electrocoagulation in the purification of a great variety of raw waters has been reported widely, e.g. for removal of dissolved arsenic from ground water and wastewater (Kumar, 2004; Parga et al., 2005), but comparatively few reports have analysed the process in detail (e.g. Chen et al., 2002). Increased efficiencies of a continuous reactor have been achieved by additional injection of air bubbles into the inlet stream, so that increased interparticle contact led to a higher flocculation rate (Parga et al., 2005). Both aluminium and iron electrodes have been used to remove up to 64% of the initial chemical oxygen demand in effluents from textile manufacture (Kobya, 2003; Can, 2006). Continuous electrocoagulation reactors with aluminium electrodes have also been used to

* Corresponding author.
Tel.: +44 207 5946121; fax: +44 207 5945934.
E-mail addresses: martin.mechelhoff@lanxess.com (M. Mechelhoff), g.kelsall@imperial.ac.uk (G.H. Kelsall), n.graham@imperial.ac.uk (N.J.D. Graham).
[1] Present address: Lanxess Deutschland GmbH, Group Function Innovation & Technology, 51369 Leverkusen, Germany.

0009-2509/$ - see front matter © 2013 Elsevier Ltd. All rights reserved.
http://dx.doi.org/10.1016/j.ces.2013.03.010

separate mineral oil from wastewater (Khemis, 2005; Carmona et al., 2006) and, using a laboratory batch reactor, to remove clay particles from aqueous dispersions (Holt et al., 2004).

A continuous single pass electrocoagulation reactor with parallel plate electrodes was used to produce potable water by removal of 96% of colour and 71% of total organic carbon (TOC) from a Norwegian surface water, using a dosage of 6 g m^{-3} aluminium(III) (Vik et al., 1984). Synthetic solutions representing natural upland water were purified of humic acid, a source of organic carbon and colour, using a laboratory electrocoagulation reactor (Jiang et al., 2002). An aluminium(III) concentration of 3.6 g m^{-3} resulted in removal of 60% of TOC and ca. 90% of colour, as opposed to 30 and 60%, respectively, when conventional coagulation methods were used with the same dosage.

However, very few publications describe the electrochemical processes occurring during electrocoagulation. One such paper (Mouedhen et al., 2008) reported aluminium anode potentials of 35 V (SCE) in sodium sulphate solution, but which decreased substantially with increasing concentrations of NaCl; no explanation for this behaviour was offered, although chloride-induced depassivation must have been responsible.

Evidently, further development and optimisation of electrocoagulation reactors can be achieved only with adequate knowledge of the electrochemical reactions and the effects of solution composition and surface chemistry, as well as topography, on aluminium dissolution rates.

A study (Heusler and Allgaier, 1971) of the oxidative dissolution kinetics of high purity aluminium electrodes in 500 mol m^{-3} sodium sulphate solutions with pH values of 9.5 to 14, enabled the derivation of pH dependent values of diffusion coefficients for dissolved aluminium(III) species. The corrosion and passivation behaviour has also been reported for high purity aluminium in solutions containing acetic acid and sodium acetate with pH values between 3.7 and 6.7 (Hurlen et al., 1984) and in 1000 mol m^{-3} NH_4Ac to which various concentrations of ammonia were added to achieve pH values between 7.2 and 9.9 (Hurlen and Haug, 1984). Tafel slopes for aluminium dissolution were found to depend on solution pH, and a relationship was developed of the potential dependence of the oxide layer thickness on aluminium electrodes for these specific experimental conditions (Hurlen et al., 1984). The kinetics of aluminium dissolution in 100 to 4000 mol m^{-3} KOH have also been reported (Brown and Whitley, 1987; Diggle and Ashok, 1976).

Recently, an extensive model (Guseva et al., 2009) of the dissolution process at a single corrosion pit on an aluminium surface in sodium chloride containing aqueous solutions predicted that hydrolysis of aluminium(III) leading to $Al(OH)^{2+}$ and releasing H^+ ions was responsible for local pH values < 3 at the bottom of the pit.

However, there is still a paucity of information about aluminium dissolution kinetics in neutral solutions of inert electrolytes, such as sodium sulphate, due to the difficulties arising from the formation of passive oxide and hydroxide for electrochemical measurements at these pH values. In addition, little is known about the effects on the dissolution process of complex organic compounds like humic acid, representing natural organic matter as one of the main contaminants in natural water.

Hence, the aims of the work for which results are reported below were to understand how dissolution of aluminium could occur in waters of pHs at which it is known to form passive oxide layers and to devise strategies for obviating such problems, enabling improved electrocoagulation process performance in purifying water from natural sources. The objectives were: (i) to determine the effects of surface pre-treatment and solution composition on aluminium oxidation and dissolution kinetics in neutral aqueous electrolyte solutions; (ii) to estimate the effective thicknesses of oxide layers from electrochemical impedance spectroscopic measurements as functions of electrode potential and applied current density. An accompanying second paper by the authors aims to explain why aluminium was found to exhibit apparent super-faradaic charge yields for its dissolution as aluminium(III), as had been reported in the literature. The apparent electron stoichiometry is required for prediction of dosing concentrations from applied currents in electrocoagulation processes.

In an electrochemical system representing an electrocoagulation reactor, the anode consists of aluminium (in our case), whereas the cathode may be made of an inert material, such as platinised titanium or stainless steel. The aluminium anode is dissolved electrochemically, but at electrode potentials $E < E_{H_2O/H_2}$, hydrogen evolution may occur in parallel:

$$j_{a,Al} \quad Al \rightarrow Al^{III} + 3e^- \tag{1}$$

$$j_{c,H_2} \quad 2H_2O + 2e^- \rightarrow H_2 + 2OH^- \tag{2}$$

Hence, the net current is

$$j_{net} = j_{a,Al} + j_{c,H_2} \tag{3}$$

At the inert cathode, hydrogen evolution by reaction (2) was considered the sole reaction at a current density j_{c,H_2}.

Due to the low solubility of Al^{III} species at neutral pH, $Al(OH)_3$ was considered to precipitate homogeneously in the bulk solution by a two-step process:

$$Al^{3+} + H_2O \underset{k_{-1}}{\overset{k_1}{\rightleftharpoons}} Al(OH)^{2+} + H^+ \tag{4}$$

$$Al(OH)^{2+} + 2H_2O \underset{k_{-2}}{\overset{k_2}{\rightleftharpoons}} Al(OH)_3 + 2H^+ \tag{5}$$

Since the solution was de-oxygenated by bubbling nitrogen (see Section 3), no current for the reduction of oxygen at the anode and cathode needed to be considered.

2. Thermodynamics of Al–H_2O systems

The superimposed potential-pH diagrams for the stable and meta-stable aluminium–water systems (Fig. 1) predict Al_2O_3 and/or (meta-stable) $Al(OH)_3$ to form in solutions of neutral pH at potentials > -2.2 V (SCE). The aqueous chemistry is more complex than implied by the list of species in Perrault (1985), as there is convincing evidence for polymeric species, the best characterised

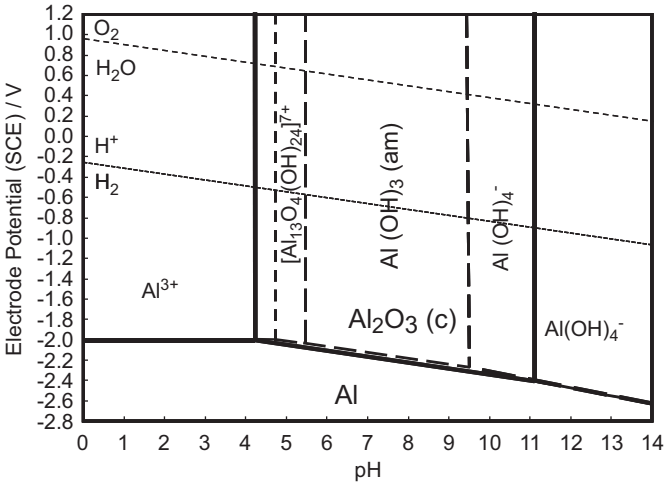

Fig. 1. Superimposed potential-pH diagrams for Al–H_2O at 298 K considering stable Al_2O_3(c) and (dashed lines) meta-stable $Al(OH)_3$ (amorphous); dissolved Al^{III} activity $= 10^{-4}$.

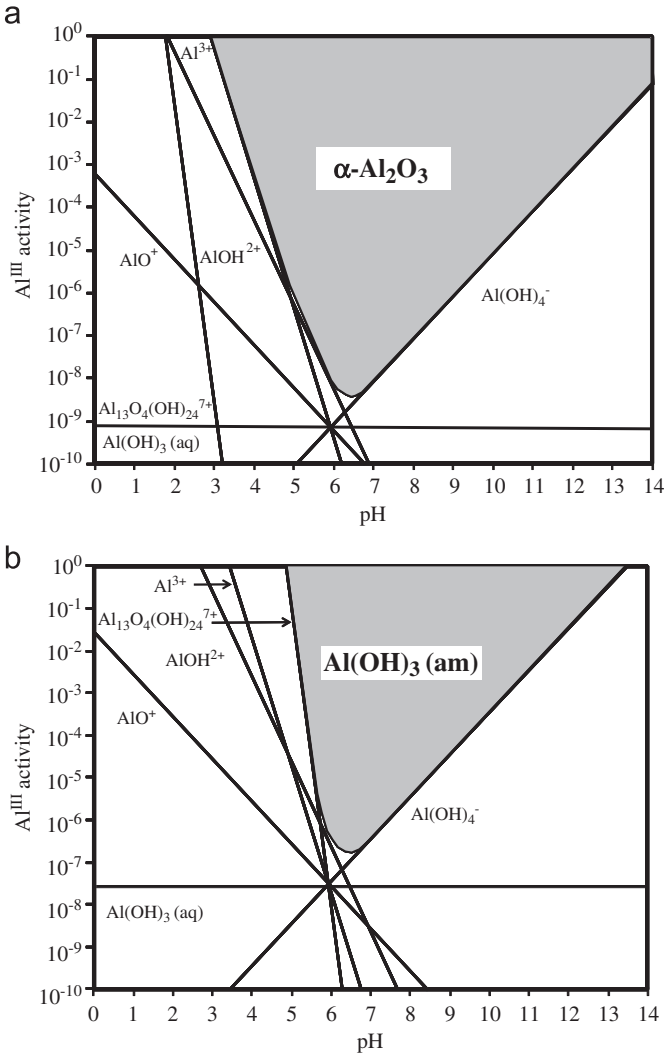

Fig. 2. (a) pH dependence of Al_2O_3(c) solubility in equilibrium with Al^{III} species at 298 K. (b) pH dependence of $Al(OH)_3$ (amorphous) solubility in equilibrium with Al^{III} species at 298 K.

(Bottero et al., 1980; Billik and Horváth, 2008; Lin and Lee, 2010) of which is $[Al_{13}O_4(OH)_{24}]^{7+}$. Its Gibbs energy of formation ($\Delta_f G^0$) of −12 372 908 J mol^{-1} was calculated from the equilibrium constant (K) (Baes and Mesmer, 1976) for the reaction:

$$13Al^{3+} + 28H_2O \leftrightarrows [Al_{13}O_4(OH)_{24}]^{7+} + 32H^+;\ \log K = -100.4 \quad (6)$$

These data were added to those listed in Perrault (1985) and used to calculate Figs. 1, 2 and 3 with a spreadsheet. For the general reaction:

$$pA_q + rH^+ + \nu_e e^- \leftrightarrows qB_p + cH_2O \quad (7)$$

$$\Delta_r G^0 = \sum_i \nu_{p,i}\Delta_f G^0\ (\text{products}) - \sum_j \nu_{r,j}\Delta_f G^0\ (\text{reactants}) = -\nu_e F E^0 \quad (8)$$

Hence,

$$E_{B/A}(\text{SHE})/V = E^0_{B/A} - \frac{0.0591r}{\nu_e}\text{pH} + \frac{0.0591}{\nu_e}\log\{c_T{}^{(p-q)}q^{-p}p^q\} \quad (9)$$

Whereas for a chemical reaction ($\nu_e = 0$):

$$\Delta_r G^0 = \sum_i \nu_{p,i}\Delta_f G^0\ (\text{products}) - \sum_j \nu_{r,j}\Delta_f G^0\ (\text{reactants}) = -\ln(10)RT\log_{10}K \quad (10)$$

For the metastable system in equilibrium with amorphous $Al(OH)_3$, $[Al_{13}O_4(OH)_{24}]^{7+}$ species were predicted to predominate

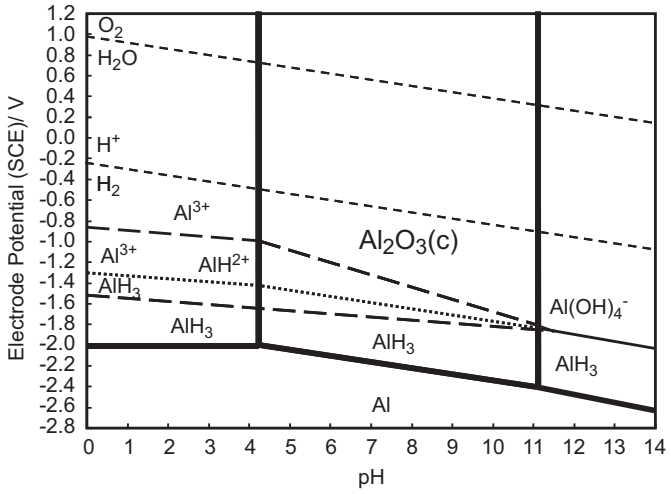

Fig. 3. Potential-pH diagram for Al–H_2O considering Al_2O_3 (c) at 298 K; dissolved aluminium activity = 10^{-4}; superimposed stability regions of (i) AlH_3 and AlH^{2+} (dashed lines) (ii) AlH_3/Al^{III} (dotted line) if AlH^{2+} does not exist.

at pH < 5.5, as shown in Fig. 2b:

$$13Al(OH)_3(am) + 7H^+ \leftrightarrows [Al_{13}O_4(OH)_{24}]^{7+} + 11H_2O \quad (11)$$

$$\log([Al_{13}O_4(OH)_{24}{}^{7+}]) = 33.82 - 7\text{pH} \quad (12)$$

Hence, the Nernst equation for the meta-stable system is plotted in Fig. 1 in the restricted pH range ca. 4.7–5.4 for a dissolved Al^{III} activity of 10^{-4}, for the reaction:

$$[Al_{13}O_4(OH)_{24}]^{7+} + 32H^+ + 39e^- \leftrightarrows 13Al + 28H_2O \quad (13)$$

$$E(\text{SCE})/V = -1.7683 - 0.0485\text{pH} + 0.0015\log([Al_{13}O_4(OH)_{24}]^{7+}) \quad (14)$$

To produce a bulk concentration (assuming concentration≈ activity) of dissolved aluminium(III) of 10^{-4} mol dm^{-3} typical of electrocoagulation processes operating with a neutral feed solution, Fig. 2a predicts that pH values < 4.7 are needed for Al^{3+} ions to be dissolved from Al_2O_3, whereas Fig. 2b predicts that pH values need to be decreased to < 5.4 to dissolve $[Al_{13}O_4(OH)_{24}]^{7+}$ ions from amorphous $Al(OH)_3$.

As suggested by Dražić and Popić (1993), aluminium may dissolve by reactions with electron stoichiometries potentially < 3; hence, greater concentrations of dissolved aluminium than implied by Eq. (1) would result at any current density. Results of aluminium electrode potential measurements as a function of pH and dissolved aluminium concentration caused Perrault to postulate the formation of dissolved aluminium hydride species, such as AlH^{2+} ions, in addition to the solid AlH_3 phase (Perrault, 1979). Corrosion due to hydrogen evolution was excluded by weight loss measurements before and after experiments, but the precision was not specified. Only the metastable $Al(OH)_3$ phase, rather than the more stable Al_2O_3 phase was included in the calculations; the relative stabilities of the two phases is evident from Fig. 2.

The potential-pH diagram(s) in Fig. 3 was calculated using Gibbs energies of formation, critically assessed by Perrault (1985), for aluminium species and phases. The diagram considering Al/Al_2O_3 phases predicted the expected solubility as Al^{3+} ions at low pH and as $Al(OH)_4^-$ ions at high pH, as in Figs. 1 and 2a. When AlH^{2+} ions and AlH_3 were included in the calculations, AlH_3 predominated over Al at low potentials, with a polygonal area of stability of AlH^{2+} ions at less negative potentials and pH less than about 11. At even less negative potentials, Al^{3+} ions were predicted to form, with Al_2O_3 then $Al(OH)_4^-$ ions predominating with increasing pH, as in Fig. 2a.

The Nernst Eq. (16) for the reaction:

$$Al + 3H^+ + 3e^- \leftrightarrows AlH_3 \ (electrochem.) \quad (15)$$

$$E_{Al/AlH_3}(SCE)/\ V = -0.604 - 0.0592pH \quad (16)$$

confirms the lack of stability of Al for any potential-pH conditions, as Al^{3+} ions $|Al_2O_3|$ $Al(OH)_4^-$ ions rather than Al would be stable at potentials predicted by Fig. 1, since the Nernst Eq. (18) for the reaction:

$$Al^{3+} + 3H^+ + 6e^- \leftrightarrows AlH_3 \ (electrochem.) \quad (17)$$

$$E_{Al^{3+}/AlH_3}(SCE)/V = -1.262 - 0.0296pH + 0.010\ \log(Al^{3+}) \quad (18)$$

corresponds to potentials more negative than those of Eq. (16).

As shown in Fig. 3, the oxidation of AlH_3 is predicted to occur at potentials greater than those given by the Nernst Eq. (20) for the reaction:

$$AlH^{2+} + 2H^+ + 4e^- \leftrightarrows AlH_3 \ (electrochem.) \quad (19)$$

$$E_{AlH^{2+}/AlH_3}(SCE)/V = -1.461 - 0.0296pH + 0.0148\ \log(AlH^{2+}) \quad (20)$$

Or at pH values > ca. 11, by the reaction:

$$Al(OH)_4^- + 7H^+ + 6e^- \leftrightarrows AlH_3 + 4H_2O \quad (21)$$

$$E_{Al(OH)_4^-/AlH_3}(SCE)/V = -1.027 - 0.069pH + 0.0099\ \log(Al(OH)_4^-) \quad (22)$$

The upper bounds of the polygon defining the stability range of AlH^{2+} ions are defined by reactions (23), (25) and (27), with corresponding Nernst Eqs. (24), (26) and (28):

$$Al^{3+} + H^+ + 2e^- \leftrightarrows AlH^{2+} \quad (23)$$

$$E_{Al^{3+}/AlH^{2+}}(SCE)/V = -0.864 - 0.0296pH + 0.0296\ \log\{(Al^{3+})/(AlH^{2+})\} \quad (24)$$

$$Al_2O_3 + 8H^+ + 4e^- \leftrightarrows 2AlH^{2+} + 3H_2O \quad (25)$$

$$E_{Al_2O_3/AlH^{2+}}(SCE)/V = -0.607 - 0.1183pH - 0.0148\ \log(AlH^{2+}) \quad (26)$$

$$Al(OH)_4^- + 5H^+ + 2e^- \leftrightarrows AlH^{2+} + 4H_2O \quad (27)$$

$$E_{Al(OH)_4^-/AlH^{2+}}(SCE)/V = -0.159 - 0.1479pH - 0.0296\ \log(AlH^{2+}) \quad (28)$$

Was Fig. 3 for the metastable system to be used to predict the kinetic behaviour of Al anodes, then active dissolution would be expected over the potential-pH range of predicted stability of AlH^{2+} ions, even if net current densities were negative due to concurrent hydrogen evolution at such potentials. Results of dissolution experiments reported previously (Holt et al., 2004; Vik et al., 1984; Jiang et al., 2002) provided no evidence of such behaviour or support for the hypothesis of the existence of AlH^{2+} ions; reversal of the sign of the net currents occurred at ca. −1.45 V (SCE) and potential-independent current densities of ca. 0.1 A m^{-2} occurred at potentials > −1.3 V (SCE), presumably due to passivation by oxide film formation.

While the thermodynamic properties (Qiu et al., 2004) and kinetic behaviour of AlH_3 are well-established, it has been reported (Adhikari and Hebert, 2008; Adhikari et al., 2010) to form at low potentials primarily at high pH > 11, as may result locally when hydrogen evolution occurs on aluminium in neutral aqueous solutions. In addition to reactions (17) and (21), reactions (29) and/or (31) and their respective Nernst Eqs. (30) and (32) define the upper potential boundary with Al^{III} species and phases

$$Al_2O_3 + 12H^+ + 12e^- \leftrightarrows 2AlH_3 \ (electrochem.) + 3H_2O \quad (29)$$

$$E_{Al_2O_3/AlH_3}(SCE)/V = -1.176 - 0.0592pH \quad (30)$$

$$Al(OH)_3 + 6H^+ + 6e^- \leftrightarrows AlH_3 \ (electrochem.) + 3H_2O \quad (31)$$

$$E_{Al(OH)_3/AlH_3}(SCE)/V = -1.190 - 0.0592pH \quad (32)$$

The issue of effective electron stoichiometry for aluminium oxide will be addressed further in the accompanying paper.

3. Experimental

An Ecochemie Autolab PGStat30 was used, which included a frequency response analysis (FRA) module, for electrochemical impedance spectroscopy. All chemicals (Na_2SO_4, NaCl and humic acid) were of reagent grade (Sigma-Aldrich). High purity water for the experiments was produced by reverse osmosis (Elga Elgastat Prima) and de-ionisation (Elga Elgastat Maxima) to give a conductivity of 1.0×10^{-6} S m^{-1}. Fresh solutions were prepared for all measurements, and were deoxygenated with high purity N_2 gas for 30 min prior to the start of an experiment, and kept under an N_2 atmosphere throughout, to prevent the ingress of atmospheric oxygen; the residual dissolved oxygen concentration was below the detection limit of a Hach-Lange dissolved oxygen electrode. No pH adjustment was carried out, so that the pH of the bulk solution was ca. 7. Due to its mildly acidic properties, a solution containing 10 g m^{-3} of humic acid had a pH of ca. 6.5.

A three compartment glass cell was used, with a saturated calomel reference electrode (Cole-Parmer) in a Luggin probe and a ca. 100 mm^2 platinum flag counter electrode (Goodfellow Ltd., UK) separated from the main compartment by a porous glass frit to prevent hydrogen bubbles from disturbing measurements.

3.1. Cyclic voltammetry

Voltammetric measurements were carried out with a rotating disc system (Pine Instruments Inc.) capable of rotation rates of 60–2000 rpm. An aluminium disc of 99.99% purity with a diameter of 5 mm formed the working electrode. Prior to each measurement it was polished wet with 50 nm alumina powder (Sigma-Aldrich) to achieve a mirror finish. After being immersed in the electrolyte solution, a potential of −2.3 V (SCE) was applied for 4 min to evolve hydrogen by reaction (2), thereby dissolving/thinning the air-formed oxide layer on the working electrode, to achieve reproducible surfaces from which to start experiments, such that subsequent behaviour was independent of electrode history.

Electrolyte solutions contained 0.5 mol m^{-3} Na_2SO_4 with the addition of 0.4 mol m^{-3} NaCl and 5 to 10 g m^{-3} humic acid, where necessary. These solutions represented the main components of the natural raw water at a typical water treatment works in West Yorkshire (UK) with typical contaminant concentrations and conductivity.

3.2. Electrochemical impedance spectroscopy

To estimate the dependence of the passive layer thickness on the applied electrode potential, impedance spectra were measured in solutions of 0.5 mol m^{-3} Na_2SO_4 with addition of 10 g m^{-3} humic acid and 0.15 mol m^{-3} NaCl at potentials typical for aluminium dissolution: −1.0, −0.6, and −0.2 V (SCE); due to the occurrence of time-dependent currents caused by pitting, −0.4 V (SCE) was applied as the final potential for the chloride containing solution. Measurements were made in a frequency range of 10^4 to

10^{-3} Hz and with an amplitude of 10 mV (p–p) (Jüttner and Lorenz, 1989; Martin et al., 2005). Only data generated at frequencies greater than 0.1 Hz were subject to fitting of an equivalent analogue circuit and are presented here, since impedances at lower frequencies did not show a dependence on applied potential and therefore were considered of no use for data analysis.

A three compartment glass electrode cell was used with a working electrode consisting of a vertical rectangular aluminium plate Al1050 (99.5% purity) of area 3.57×10^{-5} m^2 connected to a copper wire that was shrouded by a glass tube and sealed with epoxy resin at both ends, resulting in a co-planar surface with the electrode surface. Prior to each measurement, the electrode was polished to mirror finish with 50 nm alumina powder (Sigma-Aldrich), then rinsed with high purity water, immersed in 10 mol m^{-3} NaOH for 4 min, and then immersed into the measurement solution. Its potential was controlled at −2.3 V (SCE) for 5 min and at the measurement potential for 30 min before an impedance measurement was started.

3.3. Galvanostatic measurements

Two types of electrode materials were used: pure aluminium (99.99% purity; Alfa-Aesar) and technical grade aluminium 1050 (99.5%; Aldruscilla, London). In order to avoid contamination of the produced water with alloying elements, specifically pure electrode material has to be used in electrocoagulation reactors. Aluminium 1050 was the purest aluminium alloy commercially available in an industrial scale. Table 1 lists the maximum concentrations of the main impurities in Al 1050, as given by the manufacturer.

In order to provide surface conditions that were more realistic for industrial processes, the pre-treatment procedure of the working electrode was simplified compared to the impedance measurements (Section 3.2). The electrodes were prepared in two ways:

a) rough electrodes: dry polished with P1200 SiC paper (Buehler), then rinsed with high purity water.
b) smooth electrodes: dry polished with P1200 SiC paper (Buehler), then wet polished with 300 and with 50 nm alumina, finally rinsed with high purity water.

The roughness of the electrodes was measured with a Zygo white light interferometer. Table 2 lists typical roughness values for each electrode, together with the geometrical electrode area and applied current density.

Table 1
Maximum concentration of impurities in Al 1050 (Adruscilla, London).

Impurity	Cu	Si	Fe	Mn	Mg	Zn
Content limit (wt%)	0.05	0.25	0.4	0.5	0.05	0.05

Table 2
Surface roughness, electrode area and applied current density of high purity aluminium and aluminium Al 1050 used in galvanostatic experiments.

Electrode type	Pure Al 'rough'	Pure Al 'smooth'	Al1050 'rough'	Al1050 'smooth'
Purity (%)	99.99	99.99	99.5	99.5
Roughness, R_a (μm)	1.340	0.062	1.041	0.088
Electrode area (m^2)	3.9×10^{-5}	2.1×10^{-5}	3.72×10^{-5}	4.22×10^{-5}
Current density (A m^{-2})	2.56	4.76	2.69	2.37

A current of 1×10^{-4} A (≡ca. 3 A m^{-2}) was applied for 10 min during each experiment and the electrode potential recorded as a function of time. An impedance spectrum was measured at a potential of −0.55 V (SCE) in a frequency range of 1×10^{-4} Hz to 5×10^{-2} Hz before and after the current was applied. Prior to an impedance measurement, a constant potential of −0.55 V (SCE) was applied for 30 min to ensure a time-independent current signal. This potential was chosen to be above the reversible potential for hydrogen evolution $E_{H_2O/H_2} = -0.65$ V (SCE) at pH 7 and below the pitting potential $E_{pit} = -0.52$ V (SCE). Hydrogen evolution can complicate the measurement by providing a non-representative net current, whereas pitting is responsible for a time-dependent current that needs to be avoided if meaningful impedance measurements are to be obtained.

4. Results and discussion

4.1. Voltammetry at Al rotating disc electrodes

In an attempt to achieve reproducible aluminium electrode surfaces from which to start experiments, a potential of −2.3 V (SCE) was applied for 4 min to evolve hydrogen by reaction (2) after the electrode had been immersed in the electrolyte solution. Reproducible surfaces were achieved by dissolving/ thinning the air-formed oxide layer on the working electrode. Fig. 1 predicts aluminium is stable at this potential, whereas Fig. 3 predicts that the hydride phase, AlH_3, should form. Air-formed oxide and hydroxide films due to aluminium reacting with water and oxygen (Diggle and Ashok, 1976) can be dissolved chemically ('cathodically') (Azumi et al., 2004; Takahashi et al., 1994; Ogle et al., 2011) by hydroxide ions produced by reaction (2) occurring at the defects in the oxide layer at the base of pores:

$$2H_2O + 2e^-_{(Al)} \overset{k_c}{\Longrightarrow} H_2 + 2OH^-_{(x=0)} \quad \downarrow k_m \quad 2OH^-_{(x=\delta)} \tag{2}$$

coupled to:

$$Al(OH)_3(am) + OH^- \rightarrow Al(OH)_4^- \tag{33}$$

and/or:

$$Al_2O_3(c) + 3H_2O + 2OH^- \rightarrow 2Al(OH)_4^- \tag{34}$$

Depending on the applied potential, the underlying aluminium may also be oxidised, forming pits. In addition, AlH_3 (Adhikari and Hebert, 2008; Lin et al., 1994; Adhikari et al., 2008, 2010; Perrault, 1979) may have formed by e.g. reaction (15), as discussed in our accompanying paper.

Restricted rates of diffusional and migrational transport of hydroxide ions away from the base of pores with rate coefficient k_m (reaction (2)) would have caused the local pH to become alkaline, thereby dissolving (hydr-)oxide by reactions (33) and (34). Hence, in a subsequent potential scan to positive potentials, the experimental trajectory in potential-pH space would have been diagonal (Figs. 1 or 3) as the local pH relaxed towards its bulk value in the unbuffered solution with decreasing rate of reaction (2).

Fig. 4 shows a Tafel plot for a linear potential sweep between −2.3 and 0.5 V (SCE) at a rotating disc electrode; Tafel-type behaviour was evident for potentials < −1.9 V (SCE), at which hydrogen evolution was predicted by Fig. 1 to be the sole reaction, with AlH_3 formation predicted by Fig. 3. The potential of the reversal of the net current from negative to positive can be estimated from Fig. 4 as −1.45 V (SCE), corresponding to −1.70 V (SHE); this value is more positive than the equilibrium potentials for the formation of $Al(OH)_3$ and Al_2O_3, respectively, as

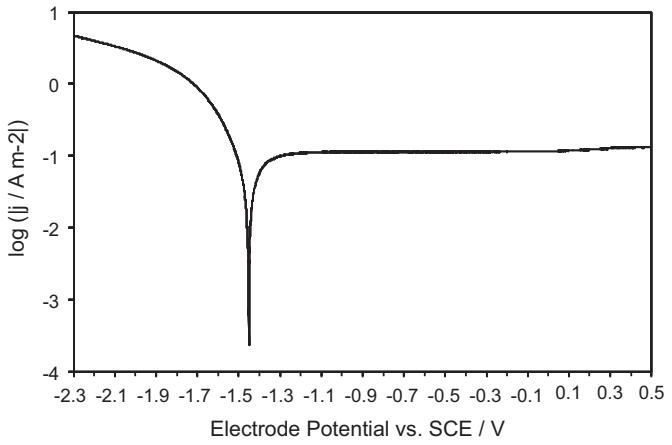

Fig. 4. Tafel plot of a linear potential sweep of a high purity aluminium disc in 0.5 mol m^{-3} Na_2SO_4; start potential: −2.3 V (SCE), end potential: 0.5 V (SCE), scan rate 1 mV s^{-1}, rotation rate: 2000 rpm.

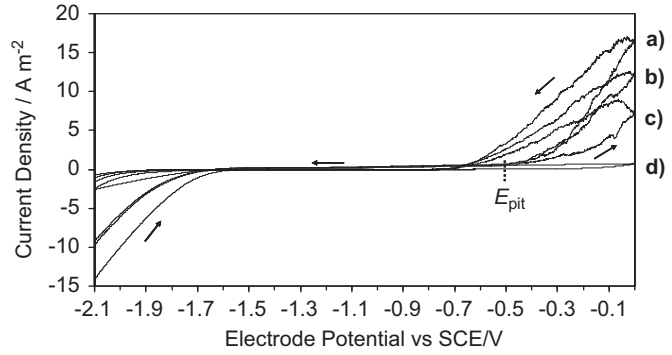

Fig. 5. Cyclic voltammogram of a high purity aluminium disc in (a) 0.5 mol m^{-3} Na_2SO_4+0.4 mol m^{-3} NaCl, (b) 0.5 mol m^{-3} Na_2SO_4+0.4 mol m^{-3} NaCl+5 g m^{-3} humic acid, (c) 0.5 mol m^{-3} Na_2SO_4+0.4 mol m^{-3} NaCl+10 g m^{-3} humic acid, (d) 0.5 mol m^{-3} Na_2SO_4; start potential: −2.1 V (SCE), vertex potential: 0.0 V (SCE), end potential: −2.1 V (SCE), scan rate 10 mV s^{-1}, rotation rate: 80 rpm.

determined by their respective Nernst equations:

$$E_{Al(OH)_3/Al}(SCE)/V = -1.717 - 0.0592pH \quad (35)$$

$$E_{Al_2O_3/Al}(SCE)/V = -1.749 - 0.0592pH \quad (36)$$

Hence, at pH 7, $E_{Al(OH)_3/Al} = -2.131$ V (SCE) and $E_{Al_2O_3/Al} = -2.163$ V (SCE), whereas the reversible potential for the evolution of hydrogen is ca. −0.65 V (SCE) at pH of 7. Therefore, at potentials between −2.1 and −0.65 V (SCE), measured current densities j_{net} (Eq. (3)) were composed of partial current densities for aluminium oxidation j_{Al} and for water reduction j_{H_2} by reaction (2). Hence, the absolute magnitude of j_{net} would have been smaller than each of its partial current densities j_{Al} and j_{H_2}, which would have been of equal magnitude at the potential corresponding to zero net current.

For potentials more positive than the reversible potentials given by Eqs. (35) and (36), passivation resulted from the formation of $Al_2O_3/Al(OH)_3$, across which most of the potential was dropped, resulting in current densities being independent of the applied potential for values more positive than −1.3 V (SCE), as evident in Fig. 4.

Humic acid and chloride ions are the main components of natural water that may affect the electrochemical behaviour of aluminium electrodes. Fig. 5 shows typical cyclic voltammograms of an aluminium electrode in solutions containing sodium sulphate, sodium chloride and humic acid, compared to the behaviour in a solution of sodium sulphate alone. On a positive-going potential scan from −2.1 V (SCE), hydrogen evolution was the predominant reaction until its reversible potential of −0.65 V (SCE), above which in pure sodium sulphate solution, current densities were very small due to passivation (Fig. 5d).

The addition of chloride ions to the sodium sulphate solution (Fig. 5a)) led to a dramatic increase in dissolution current densities for potentials > −0.52 V (SCE), due to pitting (Szklarska-Smialowska, 1986), for which chloride ions are well-known promoters. The initially increased current density on the negative-going potential sweep back from 0.0 to −2.1 V (SCE) was due to the larger surface area created by the pits. The measured pitting potential E_{pit} of −0.52 V (SCE), was close to the value of −0.49 V (SCE) reported for similar conditions (Lee, 2000). When humic acid of concentrations 5 and 10 mg dm^{-3} was added to the chloride-containing solution, the increased current densities for potentials more positive than E_{pit} were much less pronounced (Fig. 5, graphs (b) and (c)). A higher humic acid concentration resulted in decreasing oxidation current densities, though the basic behaviour and value of E_{pit} remained unchanged. Humic acids contain aromatic nuclei with carboxylic and phenolic substituents, so behave as mixtures of dibasic acids, with $pK_{a1} \approx 4$ for protonation of carboxylate groups and $pK_{a2} \approx 8$ for protonation of phenolate groups. Hence, anionic carboxylate groups would predominate at neutral pHs, so could adsorb electrostatically on positively charged aluminium oxide surfaces (p.z.c. at pH 9.1), and/or by chemisorption or chemical reaction. Hydroxy carboxylic acids (Bereket and Yurt, 2001) and sodium decanoate (Boisier et al., 2010) also have been reported to act as corrosion and pitting inhibitors for aluminium alloys.

Hence, sodium chloride is an essential for efficient dissolution of aluminium in neutral aqueous solutions, since it triggers the growth of pits that lead to dramatically increased dissolution current densities at electrode potentials greater than E_{pit}. The presence of humic acid in the solution diminishes this effect; however, complete passivation of the electrode surface caused by the adsorption of humic acid was not observed in the concentration range studied.

4.2. Effect of electrode potential on passive layer thickness

Electrochemical impedance spectroscopy was used to determine the potential dependence of the capacitance and hence the thickness of the passive oxide/hydroxide layer, together with the effects of the solution components sodium sulphate, sodium chloride and humic acid thereon.

Fig. 6 shows impedance spectra for a stationary aluminium 1050 electrode at frequencies of ca. 10^{-2}–10^{4} Hz for electrode potentials of −1.0, −0.6 and −0.2 V (SCE) in solutions containing sodium sulphate, humic acid and sodium chloride. For all potentials and in all solutions, a semi-circle was observed that overlapped with another semi-circle at lower frequencies. The radius of the semi-circles and hence the maximum imaginary impedance $-Z''_{max}$, appeared at frequencies of about 1 Hz for all measurements, and clearly increased with increasingly positive electrode potentials. In pure sulphate solution, $-Z''_{max}$ reached values in the range 0.3 to 1.5 Ω m^2, whereas addition of humic acid and sodium chloride resulted in lower values of ca. 0.35 Ω m^2 to 1.2 Ω m^2 and ca. 0.2 to 0.7 Ω m^2, respectively.

These results agree with previously published (Martin et al., 2005) impedance data for aluminium in 0.01 mol dm^{-3} NaCl, for which a slightly depressed semi-circle was found to grow in diameter with increasing applied potential, ascribed to a growing passive layer thickness.

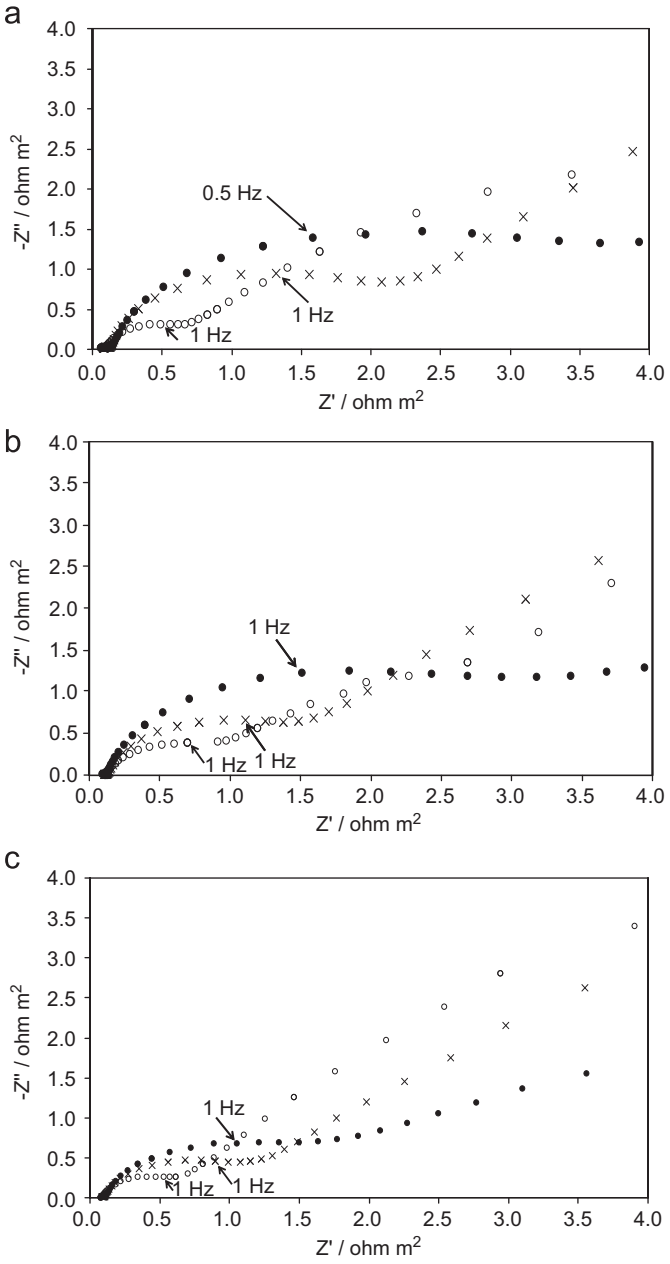

Fig. 6. Nyquist plots of electrochemical impedance of aluminium 1050 in (a) 0.5 mol m^{-3} Na_2SO_4, (b) 0.5 mol m^{-3} Na_2SO_4+10 g m^{-3} humic acid, (c) 0.5 mol m^{-3} Na_2SO_4+10 g m^{-3} humic acid+0.15 mol m^{-3} NaCl; •: −0.2 V (SCE), x: −0.6 V (SCE), ○: −1.0 V (SCE).

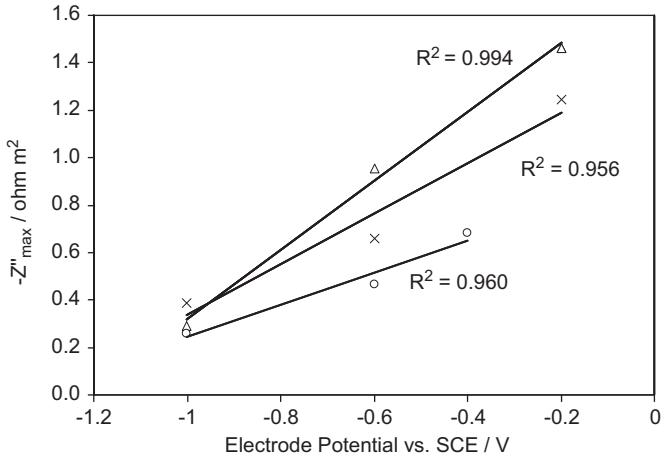

Fig. 7. Maximum imaginary impedance $-Z''_{max}$ as function of electrode potential; Δ: 0.5 mol m^{-3} Na_2SO_4, x: 0.5 mol m^{-3} Na_2SO_4+10 g m^{-3} humic acid, ○: 0.5 mol m^{-3} Na_2SO_4+10 g m^{-3} humic acid+0.15 mol m^{-3} NaCl.

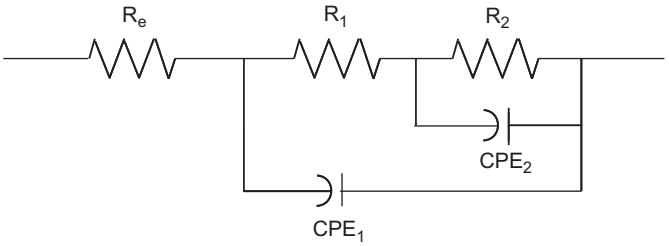

Fig. 8. Equivalent analogue electrical circuit in which (R_1 and CPE_1) and (R_2 and CPE_2) correspond respectively to porous outer and underlying barrier oxide layers, and R_e represents electrolyte resistance.

Table 3
Summary of parameter values fitted by the complex non-linear least squares (CNLS) method based on the equivalent circuit in Fig. 8 (terms as defined in Nomenclature).

Solution		0.5 mol m^{-3} sulphate		
Electrode potential (V (SCE))		−1.0	−0.6	−0.2
R_e **(ohm m²)**		1.17E+03	1.75E+03	2.78E+03
R_1 **(ohm m²)**		2.34E+03	2.62E+03	2.30E+03
R_2 **(ohm m²)**		3.25E+04	7.49E+04	1.16E+05
CPE_1	Y_0 **(ohm s^n)**	3.31E−06	1.53E−06	1.02E−06
	n	0.956	0.966	0.970
CPE_2	Y_0 **(ohm s^n)**	1.10E−05	2.39E−06	2.17E−06
	n	0.428	0.571	0.662
ω_{max} **for CPE_1 (Hz)**		1.39	1.00	0.52

The magnitude of the maximum imaginary impedance $-Z''_{max}$ was clearly dependent on the electrode potential, showing a linear increase with more positive potential. At a potential of −1.0 V, the values of $-Z''_{max}$ were similar in all solutions; however, when humic acid and sodium chloride were added, the gradient of the straight line decreased considerably, with the chloride containing solution resulting in the smallest gradient (Fig. 7). Therefore, the interfacial electrical properties of the passive layer changed, due to both humic acid and chloride ions adsorbing on the electrode surface.

The impedance data measured in pure sodium sulphate solution were fitted with a 'complex non-linear least squares' (CNLS) procedure using a program provided in the Autolab software, based on Boukamp's method (Boukamp, 2004). Having tried several possible equivalent circuits, e.g. that proposed by Jüttner and Lorenz (1989), the circuit suggested by Martin et al. (2005) proved most suitable (Fig. 8). Here, CPE_1 and R_1 refer to the porous top structure of the passive oxide layer, whereas R_2 and CPE_2 represent the properties of the underlying dense barrier layer. Pébère and Boisier (2008) suggested an identical circuit to model a porous aluminium oxide layer on aluminium AA2024 that developed during anodising in acidic solutions. However, Hitzig et al. (1984) used a slightly different circuit for a porous aluminium oxide layer, where the partial circuit R_2–CPE_2 from the model above was removed and R_e replaced with a capacitor.

Thicknesses of passive layers were estimated, based on the data listed in Table 3 resulting from fitting the experimental data to the equivalent circuit in Fig. 8. The capacitance of a constant phase element (CPE) in a parallel R–C circuit is given by (Hsu and Mansfeld, 2001)

$$C = Y_0(i\omega_{max})^{n-1} \tag{37}$$

As stated by Frers (1990) and Martin et al. (2005), the overall capacitance C comprises the partial capacitances of the passive layer C_{ox} and the Helmholtz double layer C_H. Assuming a Helmholtz capacitance of 5×10^{-1} F m^{-2} (Frers, 1990) and given the electrode area of 3.53×10^{-5} m^2, the passive layer capacitance C_{ox} can be calculated:

$$\frac{1}{C_{ox}} = \frac{1}{C} - \frac{1}{C_H} = \frac{1}{C} - \frac{1}{1.765 \times 10^{-5}\ \mathrm{F}} \tag{38}$$

This enables the estimation of the layer thickness d:

$$d = \frac{\varepsilon_r \cdot \varepsilon_0}{C_{ox}} \cdot A_e \tag{39}$$

where ε_0 denotes the vacuum permittivity ($\varepsilon_0 = 8.854 \times 10^{-12}$ F m^{-1}), ε_r the relative permittivity of aluminium oxide and A_e the electrode area. The value of the parameter ε_r was chosen as 10, based on values from the literature (Diggle and Ashok, 1976; Wolborski, 2005), though the permittivity of alumina (Al_2O_3) is extremely sensitive to its water content (Diggle and Ashok, 1976). A value of 4 was suggested for very dry γ-alumina powder, whereas Martin et al. (2005) used a value of 40 as the upper bound of their calculations for a partially hydrated passive layer. Furthermore, the permittivity also depends on the crystal structure with a value of bayerite reported as 9.4, whereas that for boehmite was measured as 20.5 (Diggle and Ashok, 1976). However, Bessone et al. (1983) used a permittivity of 9, whereas Hitzig et al. (1984) chose a value of 10. Thus, a permittivity of 10 is a reasonable estimate for a slightly hydrated oxide layer.

Fig. 9 shows a clear linear potential dependence of the layer thickness calculated for the aluminium electrode in sodium sulphate solution, as was already evident from the potential dependence of $-Z''_{max}$ values shown in Fig. 7. Linear regression of the data in Fig. 7 gave the following function:

$$d\ (\mathrm{nm}) = 1.9\ (\mathrm{nm\ V^{-1}}) \cdot \eta\ (\mathrm{V}) \tag{40}$$

The estimated passivating layer thickness increased from about 0.8 nm at −1.0 V (SCE) to ca. 2.7 nm at −0.2 V (SCE), in agreement with reported values of 0.82 nm at −1.0 V (SCE) in 0.5 mol dm^{-3} NaCl (Frers, 1990), and 1 nm at −1.0 V (SCE) in 0.1 mol dm^{-3} NaCl (Martin et al., 2005), assuming a value of 40 for the relative permittivity of aluminium oxide. For a solution of 0.16 mol dm^{-3} ammonium tartrate, a growth coefficient of 0.75 nm V^{-1} has been reported (Bessone et al., 1983) (c.f. 1.9 nm V^{-1} from Eq. (40)), with thicknesses from 0.6 nm at −1.0 V (SCE) to 1.4 nm at −0.2 V (SCE), derived using a value of 10 for the relative permittivity of aluminium oxide.

In view of the uncertainties as to the nature of the interphase formed in humic acid and chloride containing solutions, and hence in permittivity values, effective layer thicknesses were not calculated from impedance data for such solutions.

4.3. Electrode behaviour at constant current

Stationary aluminium electrodes were also used to characterise their behaviour under galvanostatic conditions. Surface preparation of the electrodes and their history, were found to have profound effects on their subsequent electrochemical behaviour. As mentioned above, electrodes were subjected to impedance measurements before and after the application of a constant current of ca. 3 A m^{-2}.

Fig. 10 shows potential-time data for a smooth aluminium 1050 electrode with a constant current of 2.37 A m^{-2} in sodium sulphate solution with no pitting promoters present, such as chloride; measurements were started immediately after the surface had been polished. Due to the growth of the passive layer on the electrode surface, the electrode potential rose linearly until the potentiostat's operational limit of the 10 V was reached. This suggests a linear growth of the passive layer; the rate of potential increase was ca. 0.054 V s^{-1}, as derived from the gradient of the line in Fig. 10.

Fig. 11 shows impedance spectra taken before and after oxidation for 600 s at 2.37 A m^{-2}. At a frequency of 8.3×10^{-2} Hz, the impedance increased from $Z' = 13$ and $-Z'' = 27\ \Omega\ \mathrm{m}^2$ before the oxidation process to $Z' = 80$ and $-Z'' = 260\ \Omega\ \mathrm{m}^2$ afterwards, due to thickening of the passive layer.

However, when the same electrode material was prepared with a rough surface finish ($R_a = 1.041$ μm) and immersed immediately in the same solution, very different potential-time data were measured, as shown in Fig. 12. Over the first 70 s, the potential increased linearly, with a slightly smaller passivation rate (0.0165 V s^{-1}) than for the smooth electrode. However, the rate of increase of potential then decelerated, with a maximum potential of ca. 1.3 V (SCE) reached after ca. 75 s, followed by a dramatic decay in potential, which stabilised at about 0.3 V (SCE) after 400 s. This was an entirely spontaneous process, caused by the increased surface roughness of the electrode compared with the behaviour of the 'smooth' electrode resulting in the data in Fig. 10, and with no pitting inducing chloride ions present in solution. Hitherto, only one recent publication has reported similar behaviour for aluminium electrodes, though in solutions containing high concentrations of sodium chloride and without providing a satisfactory explanation of this phenomenon (Mouedhen et al., 2008).

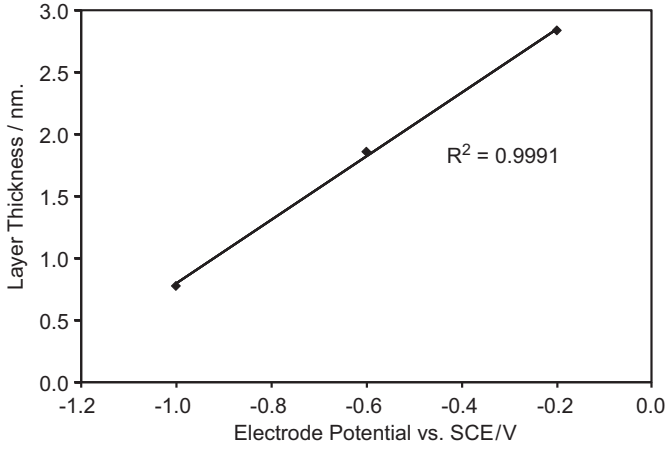

Fig. 9. Calculated passive layer thickness as function of electrode potential on aluminium Al1050 in 0.5 mol m^{-3} Na_2SO_4.

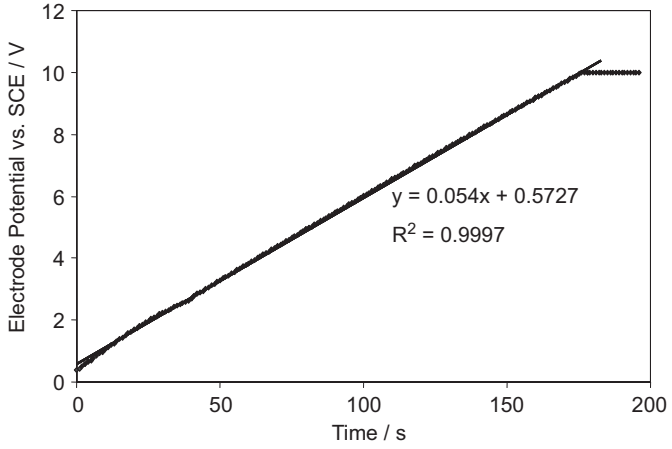

Fig. 10. Time dependence of potential of 'smooth' aluminium 1050 electrode in 0.5 mol m^{-3} Na_2SO_4; constant current density: 2.37 A m^{-2}.

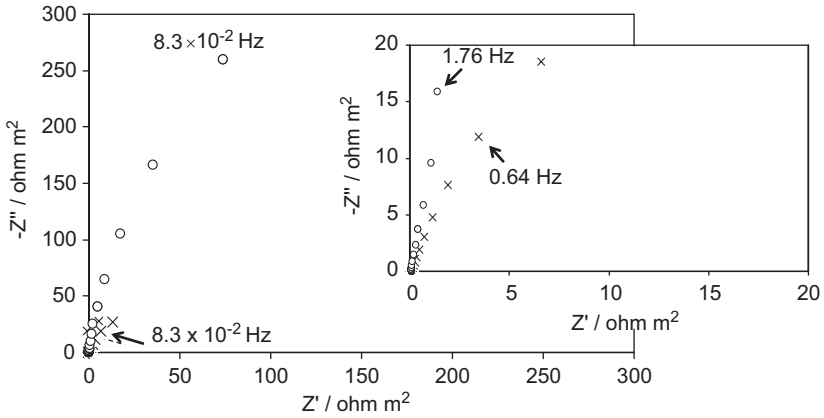

Fig. 11. Nyquist plot of electrochemical impedance spectra of 'smooth' aluminium 1050 electrode in 0.5 mol m^{-3} Na_2SO_4; x: before the dissolution process, ○: after the dissolution process, inset: impedance values at frequencies of ca. 1 Hz.

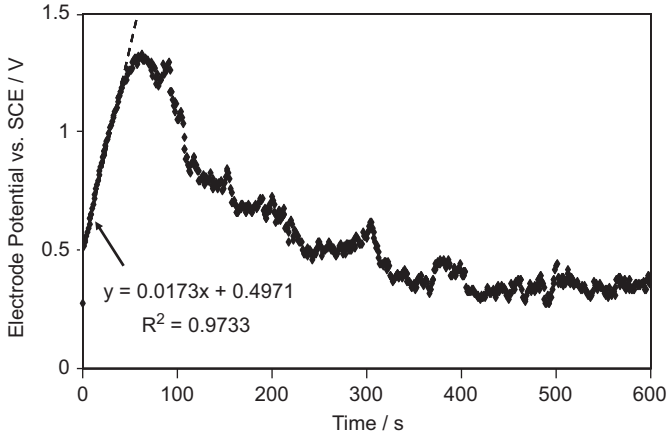

Fig. 12. Time dependence of electrode potential of 'rough' aluminium 1050 electrode in 0.5 mol m^{-3} Na_2SO_4; constant current density: 2.69 A m^{-2}.

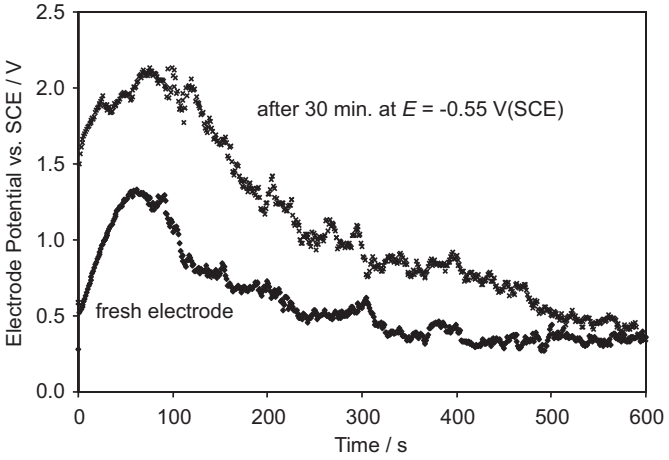

Fig. 13. Time dependence of electrode potential of 'rough' aluminium 1050 electrode in 0.5 mol m^{-3} Na_2SO_4 for a fresh surface and after 30 min at a constant potential $E=-0.55$ V (SCE); constant current density: 2.69 A m^{-2}.

From the process engineering point of view, this spontaneous de-passivation under galvanostatic control is essential for the development of an effective electrocoagulation process. It was observed for a large number of electrode types in different solutions, but with varying passivation times, rates and steady state potentials.

After the initial dissolution process, the electrode was subjected to re-passivation, by applying a constant potential of −0.55 V (SCE) for 30 min, which was followed by another dissolution process at constant current. The potential-time data after re-passivation (Fig. 13) exhibited a very similar shape to that measured for a fresh electrode surface, but the electrode potential at the start was higher due to the increased passive layer thickness caused by re-passivation. After a short passivation period, in which a peak of 2.1 V (SCE) was reached at about 100 s, the potential decayed to a steady state value of ca. 0.3 V (SCE), demonstrating that spontaneous de-passivation was reversible and reproducible, even if the surface had been subject to re-passivation.

The galvanostatic behaviour of high purity electrodes was characterised, in addition to that of aluminium 1050. Fig. 14 shows potential-time data for a smooth high purity aluminium electrode ($R_a=0.062$ μm) during the application of a constant current density of 4.76 A m^{-2}. In contrast to the behaviour of the smooth, aluminium 1050 electrode (Fig. 10), the potential increased sharply to a peak value of 1.5–1.8 V (SCE) over only a few seconds, but then decayed to a steady state value of ca. 0 V (SCE), due to spontaneous de-passivation. Thus, under these experimental conditions, high

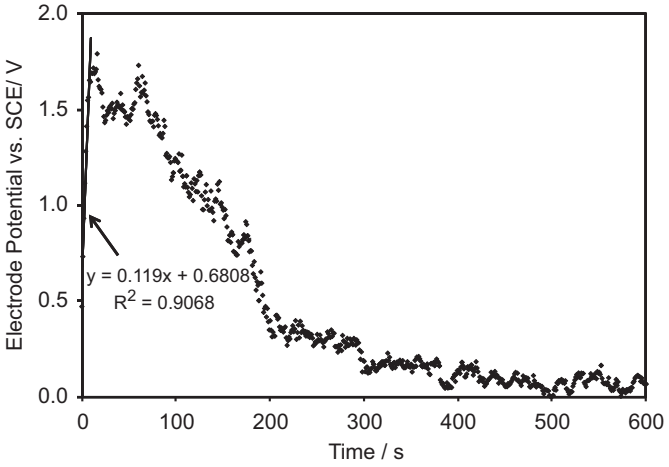

Fig. 14. Time dependence of electrode potential of 'smooth' high purity aluminium electrode in 0.5 mol m^{-3} Na_2SO_4; constant current density: 4.76 A m^{-2}.

purity electrodes are to be preferred for electrocoagulation processes, being less prone to passivation than aluminium 1050.

Fig. 15 shows impedance spectra acquired before and after oxidation at constant current density. The size of the semi-circle decreased significantly, implying a thinned passive layer.

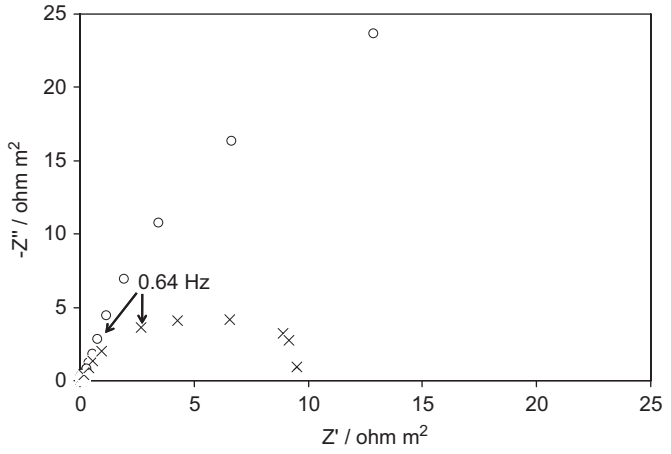

Fig. 15. Nyquist plot of electrochemical impedance spectra of 'smooth' high purity aluminium electrode in 0.5 mol m^{-3} Na_2SO_4; ○: before the dissolution process, x: after oxidation at 4.76 A m^{-2} for 600 s.

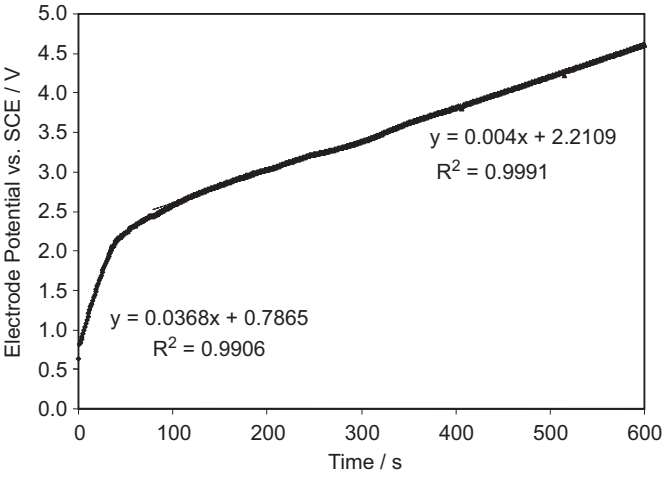

Fig. 16. Electrode potential as function of time of electrode 'rough' aluminium 1050 electrode in 0.5 mol m^{-3} Na_2SO_4 after being stored in solution for 72 h; constant current density: 2.69 A m^{-2}.

The increased depression of the post-oxidation semi-circle suggested increased surface roughness, as would be expected from an electrode surface that had undergone pitting dissolution.

In addition, the dissolution behaviour was investigated of electrodes that had been exposed to an aqueous environment at open-circuit (ca. −1.5 V (SCE)), to establish the effects of shut-down time on anodes in an electrocoagulation processes. Fig. 16 shows potential-time data for a constant current density of 2.69 A m^{-2} at a rough, aluminium 1050 electrode (R_a = 1340 μm) after it had been stored in a solution of 0.5 mol m^{-3} Na_2SO_4 for 72 h, exhibiting passivation behaviour similar to that for a freshly prepared, smooth electrode, as shown in Fig. 10. The same roughened electrode with a freshly prepared surface had previously exhibited spontaneous de-passivation, as indicated by Fig. 12. Fig. 16 shows a passivation rate of ca. 0.04 V s^{-1} for the first 35 s, similar to that of a smooth electrode, then it decelerated to a rate of 0.004 V s^{-1}, the cause of which is unclear; however, this would be congruous with the development of a more porous oxide outer layer. Apparently, hydrogen evolution and/or oxygen reduction under open circuit conditions enabled a gradual thickening of the passive layer, until it reached a critical thickness above which spontaneous de-passivation was completely inhibited, possibly due to hydrogen evolution producing hydroxide ions that dissolved the oxide film, as discussed in Section 4.4.

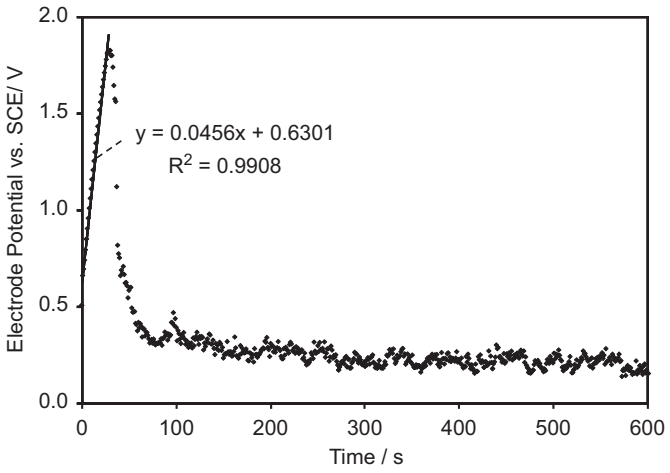

Fig. 17. Electrode potential as function of time of electrode 'rough' aluminium 1050 electrode in 0.5 mol m^{-3} Na_2SO_4 + 10 g m^{-3} humic acid + 0.15 mol m^{-3} NaCl after being stored in solution for 72 h; constant current density: 2.69 A m^{-2}.

Fig. 17 shows that after the same rough aluminium 1050 electrode was stored in a solution of 0.5 mol m^{-3} Na_2SO_4 + 0.15 mol m^{-3} NaCl + 10 g m^{-3} humic acid for 72 h, spontaneous de-passivation occurred, presumably due to the effects of chloride ions on the passive layer. The de-passivation profile was very similar to that exhibited for the same electrode with a freshly prepared surface; an initial passivation rate of ca. 0.04 V s^{-1} was observed for the first 30 s, at which the peak potential was 1.8 V (SCE), after which the potential decreased to a steady value of ca. 0.25 V (SCE).

Hence, even a relatively small concentration of chloride ions can trigger spontaneous de-passivation by promoting pitting corrosion. It is likely that these ions were incorporated into the passive film during electrode storage and thus were already present when the dissolution process started inducing spontaneous de-passivation.

4.4. Finite element reactor scale model

A two-dimensional model of the distribution of ionic and particulate species in a typical bench-scale electrocoagulation reactor was developed in Comsol Multiphysics®, version 3.4 (Modelling Guide, www.comsol.com). As outer boundary, a reactor with a rectangular structure of 0.002 × 0.15 m^2 was defined with an anode producing Al^{3+} ions by reaction (1) and a cathode evolving hydrogen by reaction (2). The homogeneous precipitation by reactions (4) and (5) was included, taking kinetic data from the literature (Holmes et al., 1968). The following three sets of equations were solved simultaneously:

i). 'Navier–Stokes' simulating laminar fluid flow at 10 dm^3 h^{-1} with the physical properties of water at 298 K:

$$\rho\frac{\partial\vec{u}}{\partial t}-\nabla\left[\eta(\nabla\vec{u}+(\nabla\vec{u})^T)\right]+\rho(\vec{u}\cdot\nabla)\vec{u}+\nabla p=\vec{F} \quad (41)$$

ii). 'Nernst–Planck' simulating the distribution of the ionic species, i, Al^{3+}, $Al(OH)^{2+}$, Na^+, SO_4^{2-}, H^+ and OH^-:

$$\nabla\cdot(-D_i\nabla c_i-z_i u_{m,i}Fc_i\nabla\phi)+\vec{u}\,\nabla c_i=R_i \quad (42)$$

iii). 'Convection and diffusion' simulating the distribution of the suspended $Al(OH)_3$ particles, formed with reaction rate R:

$$\nabla\cdot(-D\nabla c+c\vec{u})=R \quad (43)$$

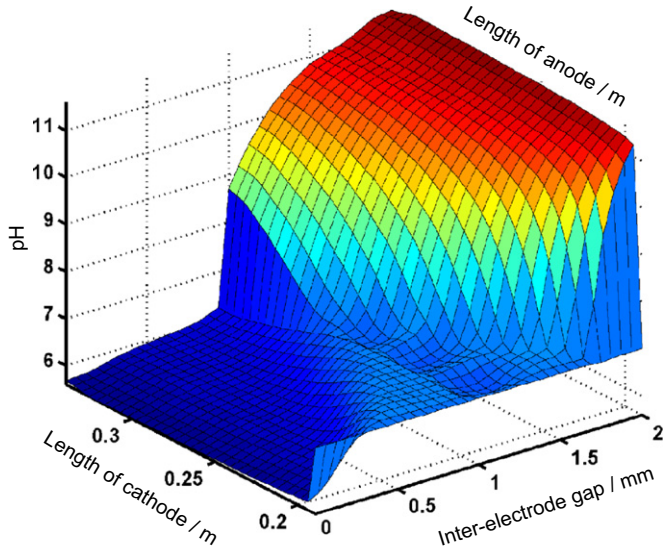

Fig. 18. Predicted pH-profile in an electrocoagulation reactor; anode: aluminium dissolution, cathode: hydrogen evolution, flow rate: 10^{-2} m^3 h^{-1}, inter-electrode gap: 2 mm, electrode length: 140 mm, electrode width: 35 mm.

In an attempt to further explain the observed spontaneous de-passivation, the finite element model was used to predict the spatial distribution of ions in a continuous electrocoagulation reactor with parallel plate electrodes.

The 'homogeneous' precipitation of aluminium forming Al$(OH)_3$ in two steps, as outlined in Section 2, was assumed to have first order kinetics. A value of 10^5 s^{-1} (Holmes et al., 1968) was used for the kinetic rate coefficient k_1 for reaction (4). No value for the rate coefficient k_2 for reaction (5) could be found in the literature, so 10^4 s^{-1} was chosen, considering the increased size of the reactant compared to the previous reaction and hence the increased probability of slower reaction kinetics. Equilibrium constants for these reactions were determined from thermodynamic data (Perrault, 1985).

An influx of water with pH 7 flowing at 2.78×10^{-6} m^3 s^{-1} (equivalent to 10 dm^3 h^{-1} or a single phase R_e=150) was applied to the model reactor, together with an anode potential of 0.4 V (SHE) or 0.155 V (SCE), which resulted in a calculated current density of 14.3 A m^{-2}. No effect of passivation was taken into account. Kinetic data for the electrochemical dissolution of aluminium (Hurlen et al., 1984) and hydrogen evolution (Dražić and Popić, 1993) reactions were taken from the literature.

Fig. 18 shows the two-dimensional spatial distribution of pH in the reactor, generated by solving Eqs. (41)–(43) using the finite element method. The pH of ca. 5.5 near the anode, due to reactions (5) and (6) releasing protons, decayed with distance to the bulk (influx) solution value of 7, from which it increased to ca. 12 near the cathode, due to hydrogen evolution by reaction (2) producing OH^- ions. Fig. 2b predicts that a pH of ca. 5.5 would enable spontaneous dissolution of Al$(OH)_3$ as $[Al_{13}O_4(OH)_{24}]^{7+}$ ions.

The low pH at the anode facilitates aluminium dissolution, dissolving pre-existing oxide and postponing aluminium hydrolysis and (hydrous)oxide formation, which occurs progressively as Al^{3+} ions are transported towards the bulk solution mainly by convective diffusion. This explains the relatively low steady state electrode potential and feasibility of electrocoagulation process for influents with neutral pH, at which Fig. 1 predicts passivation.

5. Conclusions

Aluminium tends to passivate in neutral electrolyte solutions, resulting in very small dissolution current densities over a wide potential range. It was shown that the thickness of the passive layer grows linearly with increasingly positive electrode potentials. The presence of natural contaminants, such as humic acid, exacerbates the problem, which is detrimental to the performance of electrocoagulation reactors, for which a constant dosage of dissolved aluminium(III) and a minimal energy demand is required. However, the effects of passivation can be diminished by adding pitting promoters, such as chloride ions, to the electrolyte solution, though such chemical additions would increase the complexity and costs of electrocoagulation processes, so are not the preferred option to achieve performance improvements.

In the experiments reported here, a constant current was applied that caused a smooth aluminium electrode to exhibit passivation behaviour resulting in a constantly increasing anode potential, cell voltage and hence specific electrical energy consumption, threatening the technical and economic viability of any electrocoagulation process. However, when the electrode surface was roughened, the electrode potential decreased dramatically to a low and steady value. This effect of 'spontaneous de-passivation' was observed even without the presence of chloride ions. Exposing the electrode at open circuit to an electrolyte solution for long times reversed the effect. It can be attributed to the hydrolysis of dissolved aluminium(III) ions close to the electrode surface releasing protons, which dissolve the pre-existing passive layer and enhance dissolution rates. Apparently, this dissolution process is facilitated by cracks in the passivating layer of the rough electrode surface.

Hence, contrary to common perception, it is possible to dissolve aluminium electrochemically at neutral pH without the addition of pitting promoters just by simply roughening the electrode surface. It can be concluded that the electrocoagulation treatment of natural waters containing none or very low concentrations of chloride just requires a freshly roughened aluminium electrode surface, which may improve the technical and economic viability of electrocoagulation processes significantly. Further research is still required to better understand the process of spontaneous de-passivation.

Nomenclature

A_e	Electrode area (m^2)
c	Concentration (mol m^{-3})
C	Area specific capacitance (F m^{-2})
d	Passive layer thickness (m)
D	Diffusion coefficient (m^2 s^{-1})
E	Electrode potential vs. reference electrode (V)
E_{eqm}	Equilibrium potential vs. reference electrode (V)
F	Faraday constant, 96,485 (C mol^{-1})
$\vec{F}$	Volume force field (N m^{-3})
j	Current density (A m^{-2})
j_0	Exchange current density (A m^{-2})
K	Equilibrium constant
k_i	Standard rate coefficient for reaction i (m s^{-1})
n	Exponent in Eq. (37); $n=1/(D-1)$, where D is the fractal dimension (1)
p	Pressure (Pa)
R	Gas constant, 8.314472 (J mol^{-1} K^{-1})
R	Reaction rate (mol m^{-3} s^{-1})
R_a	Degree of surface roughness (μm)
SHE	Standard hydrogen electrode (dimensionless)
t	Time (s)
T	Temperature (K)
$u_{m,i}$	Ionic mobility (Eq. (42)) (m^2 mol J^{-1} s^{-1})
$\vec{u}$	Velocity (m s^{-1})
Y_0	Area specific admittance (Eq. 37) (F s^{1-n} m^{-2})

z	Electron stoichiometric factor/reaction charge number (1)
Z'	Impedance, real part ($\Omega\ m^2$)
Z''	Impedance, imaginary part ($\Omega\ m^2$)
$\Delta_f G_i^0$	Gibbs energy of formation of species i ($J\ mol^{-1}$)
$\Delta_r G^0$	Gibbs energy of formation of reaction ($J\ mol^{-1}$)
ε	Permittivity ($F\ m^{-1}$)
ε_r	Relative permittivity (1)
ϕ	Potential (V)
η	Overpotential, (E–E_{eqm}) (Eq. (40)) (V)
η	Dynamic viscosity (Eq. (41)) (Pa s)
ν	Stoichiometric number (1)
ν_e	Electron stoichiometric number of reaction (1)
ρ	Density of electrolyte solution ($g\ m^{-3}$)
ρ_{Al}	Density of aluminium ($g\ m^{-3}$)
ω	Angular frequency ($rad\ s^{-}$)[1]

Acknowledgements

The authors thank Yorkshire Water, Bradford (UK), for funding this project.

References

Adhikari, S., Hebert, K.R., 2008. Participation of aluminium hydride in the anodic dissolution of aluminium in alkaline solutions. J. Electrochem. Soc. 155 (5), C189–C195.
Adhikari, S., Lee, J., Hebert, K.R., 2008. Formation of aluminium hydride during alkaline dissolution of aluminium. J. Electrochem. Soc. 155 (1), C16–C21.
Adhikari, S., Ai, J., Hebert, K.R., Ho, K.M., Wang, C.Z., 2010. Hydrogen in aluminium during alkaline corrosion. Electrochim. Acta 55 (19), 5326–5331.
Azumi, K., Ueno, T., Seo, M., 2004. Cathodic dissolution behaviour of an aluminium wire electrode in solutions containing borate and sulphate ions. J. Electroanal. Chem. 567 (1), 1–7.
Baes Jr., C.F., Mesmer, R.E., 1976. The Hydrolysis of Cations. Wiley, New York.
Bereket, G., Yurt, A., 2001. The inhibition effect of amino acids and hydroxy carboxylic acids on pitting corrosion of aluminium alloy 7075. Corros. Sci. 43 (6), 1179–1195.
Bessone, J., Mayer, C., Jüttner, K., Lorenz, W.J., 1983. AC-impedance measurements on aluminium barrier type oxide films. Electrochim. Acta 28 (2), 171–175.
Billik, P., Horváth, B., 2008. Mechanochemical synthesis of the $[Al_{13}O_4(OH)_{24}(H_2O)_{12}]^{7+}$ Keggin ion. Inorg. Chem. Commun. 11 (10), 1125–1127.
Boisier, G., Portail, N., Pébère, N., 2010. Corrosion inhibition of 2024 aluminium alloy by sodium decanoate. Electrochim. Acta 55 (21), 6182–6189.
Bottero, J.Y., Cases, J.M., Fiessinger, F., Poirier, J.E., 1980. Studies of hydrolyzed aluminium chloride solutions. 1. Nature of aluminium species and composition of aqueous solutions. J. Phys. Chem. 84 (22), 2933–2939.
Boukamp, B.A., 2004. Electrochemical impedance spectroscopy in solid state ionics: recent advances. Solid State Ionics 169 (1-4), 65–73.
Brown, O.R., Whitley, J.S., 1987. Electrochemical behaviour of aluminium in aqueous caustic solutions. Electrochim. Acta 32 (4), 545–556.
Can, O.T., 2006. Treatment of the textile wastewater by combined electrocoagulation. Chemosphere 62, 181–187.
Carmona, M., Khemis, M., Leclerc, J-P., Lapicque, F., 2006. A simple model to predict the removal of oil suspensions from water using the electrocoagulation technique. Chem. Eng. Sci. 61, 1237–1246.
Chen, X., Chen, G., Yue, P.L., 2002. Investigation on the electrolysis voltage of electrocoagulation. Chem. Eng. Sci. 57, 2449–2455.
Diggle, J.W., Ashok, K.V., 1976. Oxides and Oxide Films. Marcel Dekker, New York.
Dražić, D., Popić, J., 1993. Hydrogen evolution on aluminium in chloride solutions. J. Electroanal. Chem. 357 (1–2), 105–116.
Frers, S.E., 1990. AC-Impedance measurements on aluminum in chloride containing solution and below the pitting potential. J. Appl. Electrochem. 20 (6), 996–999.
Guseva, O., Schmitz, P., Suter, T., von Trzebiatowski, O., 2009. Modelling of anodic dissolution of pure aluminium in sodium chloride. Electrochim. Acta 54 (19), 4514–4524.
Heusler, K.E., Allgaier, W., 1971. Die kinetik der aufloesung von aluminium in alkalischen loesungen. Werkst. Korros. 4, 297–302.
Hitzig, J., Jüttner, K., Lorenz, W.J., Paatsch, W., 1984. AC-Impedance measurements on porous aluminium oxide films. Corros. Sci. 24 (11-12), 945–952.
Holmes, L.P., Cole, D.L., Eyring, E.M., 1968. Kinetics of aluminium ion hydrolysis in dilute solutions. J. Phys. Chem. 72 (1), 301–304.
Holt, P.K., Barton, G.W., Mitchell, C.A., 2004. Deciphering the science behind electrocoagulation remove suspended clay particles from water. Water Sci. Technol. 50 (12), 177–184.
Hsu, C.H., Mansfeld, F., 2001. Technical note: concerning the conversion of the constant phase element parameter Y-0 into a capacitance. Corrosion 57 (9), 747–748.
Hurlen, T., Haug, A.T., 1984. Corrosion and passive behaviour of aluminium in weakly alkaline solution. Electrochim. Acta 29 (8), 1133–1138.
Hurlen, T., Lian, H., Ødegard, O.S., 1984. Corrosion and passive behaviour of aluminium in weakly acid solution. Electrochim. Acta 29 (5), 579–585.
Jiang, J.Q., Graham, N.J.D., Kelsall, G.H., Brandon, N.P., 2002. Laboratory study of electro-coagulation-flotation for water treatment. Water Res. 36, 4064–4078.
Jüttner, K., Lorenz, W.J., 1989. The role of surface inhomogeneities in corrosion processes. Electrochemical impedance spectroscopy (EIS) on different aluminum-oxide films. Corros. Sci. 29 (2-3), 279–288.
Khemis, M., 2005. Electrocoagulation for the treatment of oil suspensions relation between the rates of electrode reactions and the efficiency of waste removal. Process Saf. Environ. Prot. 83 (B1), 50–57.
Kobya, M., 2003. Treatment of textile wastewaters by electrocoagulation using iron and aluminum electrodes. J. Hazardous Mater. 100, 163–178.
Kumar, P.R., 2004. Removal of arsenic from water by electrocoagulation. Chemosphere 55, 1245–1252.
Lee, W.J., 2000. Effects of sulphate ion additives on the pitting corrosion of pure aluminium in 0.01 M NaCl solution. Electrochim. Acta 45 (12), 1901–1910.
Lin, C-F., Porter, M.D., Hebert, K.R., 1994. Surface films produced by cathodic polarization of aluminium. J. Electrochem. Soc. 141 (1), 96–104.
Lin, Y-F., Lee, D-J., 2010. Purification of aluminium tridecamer salt using organic solvent precipitation. Sep. Purif. Technol. 75 (2), 218–221.
Martin, F.J., Cheek, G.T., O'Grady, W.E., Natishan, P.M., 2005. Impedance studies of the passive film on aluminium. Corros. Sci. 47 (12), 3187–3201.
Mouedhen, G., Feki, M., Wery, De Petris, Ayedi, H.F., M., 2008. Behavior of aluminum electrodes in electrocoagulation process. J. Hazardous Mater. 150 (1), 124–135.
Ogle, K., Serdechnova, M., Mokaddem, M., Volovitch, P., 2011. The cathodic dissolution of Al, Al2Cu, and Al alloys. Electrochim. Acta 56 (4), 1711–1718.
Parga, J.R., Cocke, D.L., Valenzuela, J.L., Gomes, J.A., Kesmez, M., Irwin, G., Moreno, H., Weir, M., 2005. Arsenic removal via electrocoagulation from heavy metal contaminated groundwater in La Comarca Lagunera Mexico. J. Hazardous Mater. 124, 247–254.
Pébère, N., Boisier, G., 2008. EIS study of sealed AA2024 anodized in sulphuric acid solutions. In: Proceedings of the 213th Meeting of the Electrochemical Society, Phoenix, AZ, 18–23 May 2008, The Electrochemical Society, Abstract 906.
Perrault, G.G., 1979. The role of hydrides in the equilibrium of aluminium in aqueous solutions. J. Electrochem. Soc. 126 (2), 199–204.
Perrault, G.G., 1985. In: Bard, A.J., Parsons, R., Jordan, J. (Eds.), Standard Potentials in Aqueous Solutions. Marcel Dekker, New York, pp. 555–580.
Qiu, C., Olson, G.B., Opalka, S.M., Anton, D.L., 2004. Thermodynamic evaluation of the Al-H system. J. Phase Equilibria Diffusion 25 (6), 520–527.
Szklarska-Smialowska, Z., 1986. Pitting Corrosion of Metals. National Association of Corrosion Engineers, Houston, TX.
Takahashi, H., Fujiwara, K., Seo, M., 1994. The cathodic polarization of aluminium covered with anodic oxide films in a neutral borate solution—II. Film breakdown and pit formation. Corros. Sci. 36 (4), 689–705.
Vik, E.A., Carlson, D.A., Eikum, A.S., Gjessing, E.T., 1984. Electrocoagulation of potable water. Water Res. 18 (11), 1355–1360.
Wolborski, M., 2005. Characterization of aluminum and titanium oxides deposited on 4H SiC by atomic layer deposition technique. Mater. Sci. Forum 483, 701–704.